

Rapid edge-plasma prediction in the W7-X standard configuration from experimental diagnostics via neural-network surrogates

Y. Luo^{1,2*}, S. Xu¹, Y. Liang^{1,2}, E. Wang¹, J. Cai¹, A. Knieps¹, P. Ren^{1,2}, M. Tan^{1,2}, Y. Feng³, D. Reiter², S. Brezinsek^{1,2}, D. Harting¹, M. Krychowiak³, D. Gradic³, D. Zhang³, Y. Gao³, G. Fuchert³, A. Pandey³, M. Jakubowski³ and the W7-X Team

¹ *Forschungszentrum Jülich GmbH, Institute of Fusion Energy and Nuclear Waste Management – Plasma Physics, 52425 Jülich, Germany*

² *Faculty of Mathematics and Natural Science, Heinrich Heine University Düsseldorf, 40225 Düsseldorf, Germany*

³ *Max Planck Institute for Plasma Physics, 17491 Greifswald, Germany*

This study aims to develop an end-to-end neural surrogate, EMC3-EIRENE-AI, that predicts full 3D edge plasma parameter distributions consistent with the EMC3-EIRENE model directly from routine edge-diagnostic measurements and their uncertainties, delivering results on an office desktop in just seconds to a few minutes. The system couples two neural components: (i) a Bayesian neural network that infers EMC3-EIRENE input parameters directly from routine diagnostic measurements in a way that is statistically consistent with those diagnostics; and (ii) a neural surrogate model that maps EMC3-EIRENE input parameters to the corresponding full EMC3-EIRENE outputs. Compared with the traditional trial-and-error adjustment of EMC3-EIRENE inputs to match diagnostics—each run demanding thousands of CPU-core-hours—EMC3-EIRENE-AI reduces both human effort and computing time while providing results that are statistically consistent with measurements and their uncertainties, enabling rapid scenario exploration and integration into larger multi-physics modelling chains.

1. Introduction

Edge plasma transport modelling is important to understanding boundary plasma behaviour and to optimizing the design and operation of magnetic-confinement fusion devices. The challenge is amplified in configurations with intrinsically three-dimensional edge topology—such as the Wendelstein 7-X (W7-X) stellarator—where boundary diagnostics measure only localized regions, complicating inverse inference of global transport. The EMC3-EIRENE code is well suited to such geometries and has been extensively applied in both tokamaks and stellarators for interpreting experiments and performing predictive studies [1-8]. However, bringing EMC3-EIRENE simulations into quantitative agreement with diagnostic measurements typically demands laborious, manual adjustment of uncertain input parameters—especially cross-field transport coefficients—and multiple forward runs. Each candidate run is compared to experimental data until an acceptable match is reached, a workflow that is both time-consuming and computationally expensive. Fortunately, data-driven neural-network surrogate offers a promising solution.

2. Data generation and workflow

A dedicated database was generated with the EMC3-EIRENE code. In all simulations carbon sputtered from divertor targets or baffles was prescribed as the sole radiation source; its effective source strength was regulated via the

Table 1: Range of EMC3-EIRENE input parameters.

Parameters	Ranges								
P_{in} (MW)	4	6	8	10					
f_{rad}	0.2	0.4	0.6	0.8					
$n_{e,sep}$ (10^{19} m^{-3})	2	3	3.5	4	4.5	5	5.5	6	7
D_{\perp} (m^2/s)	0.1	0.3	0.5	0.7	0.9	1.1	1.5	2	
χ_{\perp} (m^2/s)	0.2	0.6	0.9	1.2	1.5				

imposed total radiated power. Cross-field particle diffusivities for hydrogen (bulk plasma) and carbon were taken to be equal and spatially uniform, as were the electron and ion thermal diffusivities. Five primary input parameters were systematically scanned for the W7-X standard magnetic configuration: input heating power across the innermost boundary surface (P_{in}), radiation power fraction (f_{rad}), electron density at the separatrix ($n_{e,sep}$), cross-field particle diffusivity D_{\perp} and cross-field thermal diffusivity χ_{\perp} . Parameter ranges (Table 1) were chosen to span the typical operational window of W7-X in this configuration. An exhaustive grid over the full Cartesian product of values in Table 1 would be computationally prohibitive and unnecessarily dense. Empirically, beyond a certain database size, additional samples yielded only marginal surrogate improvements. We therefore drew 463 input sets at random (stratified over the allowed ranges) and executed each to numerical convergence with EMC3-EIRENE, forming the converged-simulation database used for training and inference.

To enable prediction of full 3D edge plasma profiles directly from routine diagnostics, we introduce EMC3-EIRENE-AI. As outlined in Figure 1, the workflow has two stages: 1. a Bayesian neural network that infers EMC3-EIRENE input parameters from diagnostics. 2. a forward surrogate that maps those inputs to EMC3-EIRENE output profiles. Both networks are trained on the same simulation database; they differ only in mapping direction. Each measurement enters with an uncertainty estimate and a prior distribution for its associated EMC3-EIRENE input

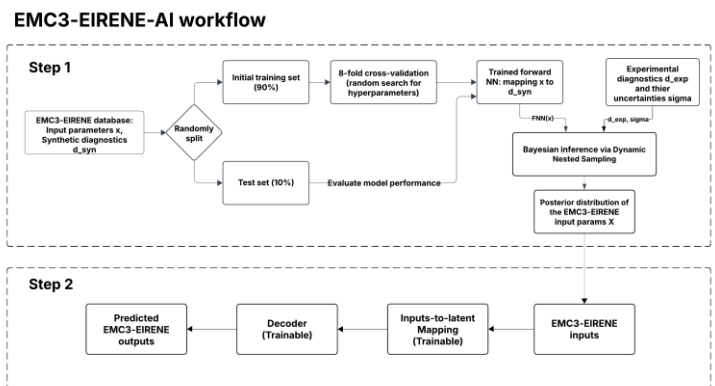


Figure 1: Two-step EMC3-EIRENE-AI workflow for Bayesian input inference and fast surrogate output prediction.

those inputs to EMC3-EIRENE output profiles. Both networks are trained on the same simulation database; they differ only in mapping direction. Each measurement enters with an uncertainty estimate and a prior distribution for its associated EMC3-EIRENE input

parameters, enabling uncertainty-aware inversion in step 1.

To demonstrate practical application, we analyze W7-X density-ramp discharge #20181010.028. Figure 2 presents principal plasma traces for this shot, which evolves toward divertor detachment. Three time slices are selected, spanning distinct radiation fractions: $f_{rad}(t1) = 0.2$, $f_{rad}(t2) = 0.5$, and $f_{rad}(t3) = 0.8$. For each slice—capturing both upstream and divertor conditions—we supply the following edge-diagnostic set to the framework: divertor C II line emission profile from divertor spectroscopy, Thomson scattering (TS) radial profiles of electron density and temperature, ion saturation currents from divertor Langmuir probes (LPs) and divertor heat-flux profiles from infrared thermography. From these inputs, EMC3-EIRENE-AI returns self-consistent 3D edge plasma parameters, enabling the application cases outlined in the subsequent subsections.

3. Application of the EMC3-EIRENE-AI

We now present several applications of EMC3-EIRENE-AI.

Fast transport analysis: Figure 3 shows the time evolution of the inferred cross-field particle diffusivity D_{\perp} (blue) and thermal diffusivity χ_{\perp} (red). As the radiated power fraction increases and the plasma evolves from low to high recycling, both coefficients rise. A sharp drop in χ_{\perp} occurs near $t \approx 3$ s; D_{\perp} decreases abruptly around $t \approx 5.0$ s. During the subsequent transition toward detachment both climb slightly, then fall again once divertor gas puffing ends, accompanied by radiation reduction.

Boundary-regime evaluation: Figure 4 gives the predicted recycling flux (orange) together with the measured radiation fraction $f_{rad,exp}$ (cyan). The flux increases with $f_{rad,exp}$ until a rollover at $f_{rad,exp} \approx 0.45$, indicating the onset of detachment. With further radiation

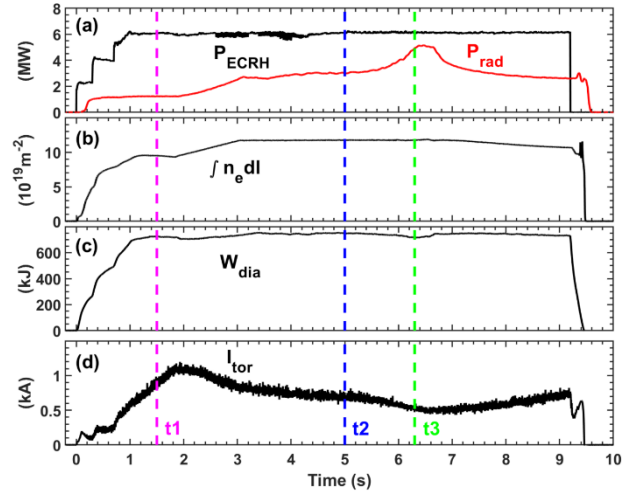


Figure 2: Temporal evolution of key signals for the density-ramp discharge #20181010.028 on W7-X.

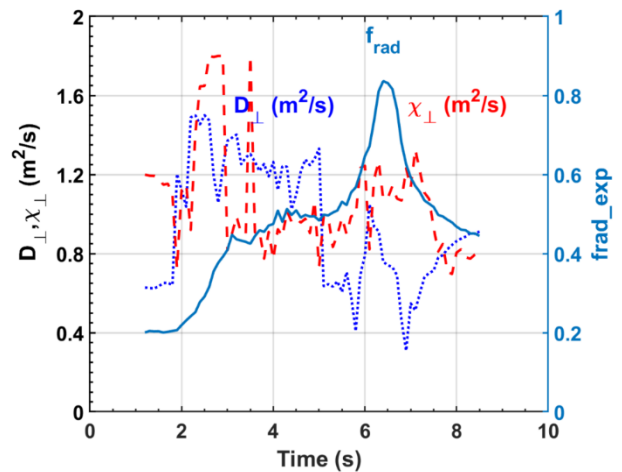


Figure 3: Variation of the inferred cross-field transport coefficients with time.

rise it declines, then drops rapidly in deep detachment. After gas puff termination, $f_{rad,exp}$ decreases and the recycling flux rebounds. For this 6 MW ECRH discharge the high-recycling to detachment threshold is therefore $f_{rad,exp} \approx 0.45$, providing a practical control reference.

Real-time mapping: The framework converts diagnostics directly into full 3D edge plasma parameter profiles. Figures 5 compare electron temperature and impurity radiation at the three time slices in Figure 2 ($f_{rad} = 0.2, 0.5, 0.8$). Increasing f_{rad} cools the SOL, especially near the magnetic island, driven by deeper impurity penetration. At low radiation, intense emission is localized near strike points. By $f_{rad} \approx 0.5$, radiation strengthens and extends upstream. At $f_{rad} \approx 0.8$ (detachment), the main radiation front shifts into the SOL and advances toward the separatrix, where a pronounced peak forms as detachment deepens.

4. Summary

In this work, we introduced EMC3-EIRENE-AI, enabling rapid edge transport analysis directly from routine diagnostics (with uncertainties). From measured signals it (i) performs Bayesian inference of the EMC3-EIRENE input parameters consistent with the data, then (ii) uses a forward surrogate to produce full 3D EMC3-EIRENE outputs. The next step is to integrate this loop with feedback control, coupling edge diagnostics, physics-based modelling, and supervisory decision support for sustained high-power W7-X operation.

References

- [1] F. Effenberg et al., Nucl Fusion 57 (2017).
- [2] S. Xu et al., Nucl Fusion 58 (2018).
- [3] S. Xu et al., Nucl Fusion 60 (2020).
- [4] Y. Feng et al., Nucl Fusion 61 (2021).
- [5] S. Xu et al., Nucl Fusion 63, 066005 (2023).
- [6] V. R. Winters et al., Nucl Fusion 64 (2024).
- [7] Y. Feng et al., Nucl Fusion 64 (2024).
- [8] V. R. Winters et al., Nucl Fusion 64 (2024).

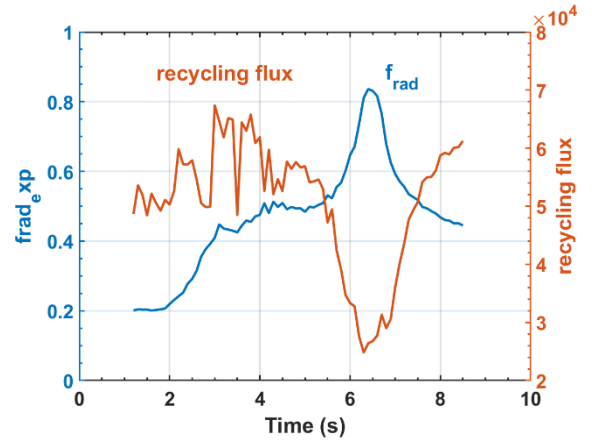


Figure 4: Evolution of the recycling flux during the radiation ramp.

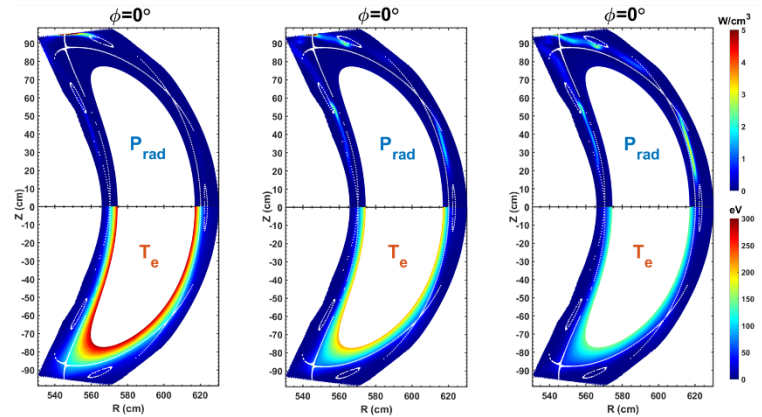


Figure 5: Radiation power and electron temperature contours in the bean-shaped cross-section predicted by EMC3-EIRENE-AI.